

Influence of cooling rate on crystallisation kinetics on microstructure of cast zinc alloys

Mariusz Krupiński · Beata Krupińska ·
Krzysztof Labisz · Zbigniew Rdzawski ·
Wojciech Borek

Received: 13 March 2014 / Accepted: 12 September 2014 / Published online: 7 October 2014
© The Author(s) 2014. This article is published with open access at Springerlink.com

Abstract In this study, the change of the cooling rate in the range of about $0.1\text{--}1\text{ }^{\circ}\text{C s}^{-1}$ and the addition of Sr on the crystallization kinetics of the cast zinc alloys of the ZnAlCu type, as well as its relation to the microstructure were also investigated. Therefore, the aim of the rapid crystallisation is the achievement of materials with better properties, which can be obtained by refinement of the dendritic or eutectic microstructure, elimination of segregation, or creation of metastable phases and their morphology changes. In the investigated alloys, the change of cooling rate of $1\text{ }^{\circ}\text{C s}^{-1}$ has caused microstructure's refinement as well as increase in hardness. Increase in the cooling rate causes also morphology changes of the $\eta + \alpha$ eutectic, and makes generally a global overcooling of the alloy as well as change in the temperatures at the beginning of crystallization T_{DN} and of the alloy crystallization T_{S} . The presented investigations concerning the electron microscopy methods, including transmission electron microscopy, allow revealing the crystallographic structure, based on the d-spacing changes, as well as the diffraction method used for phase determination, which is a helpful tool for the explanation of the important points in the thermo-derivative analysis curve, where the relation between the amount of phase and the occurrence of new phases can be determined.

Keywords Zinc alloy · Microstructure · Thermo derivative analysis · Crystallisation kinetics · Phase composition

Introduction

Properties of zinc cast alloys, including corrosion resistance, accompanied, however, by low or high mechanical properties, predispose the copper zinc alloys for use in an environment with increased susceptibility to corrosion. These functional properties can be modified by changing the chemical composition and cooling rate, which very strongly influences the microstructure. Inoculation or modification takes place if the total of the modifiers does not exceed 1 mass %; in this case, the amount of the additives is even higher, and so no modification is carried out, except an addition of the special alloying additives like those usable for inoculation. This was done to investigate the influence of the additives of different amounts used between a real modification and alloying elements addition. Very important are also the technological factors, such as temperature of the metal bath and the system composed of the metal and the mould, which determine the changes that occurred in the material (the dissolution of alloying elements and the formation of eutectic phases, as well as the specific heat and heat transfer in the casting system) [1, 2].

The progress of technology requires the use of modern engineering materials with improved functional properties, which at the same time, is expected to increase the quality and efficiency of production due to the increasing competition in the market, leading to reduction in production costs. There is also a need to look for cost savings at the level of production quality control. The aim is to increase

M. Krupiński (✉) · B. Krupińska · K. Labisz · Z. Rdzawski ·
W. Borek
Division of Constructional and Special Materials, Institute of
Engineering Materials and Biomaterials, Silesian University of
Technology, Konarskiego Str 18A, 44-100 Gliwice, Poland
e-mail: Mariusz.Krupinski@polsl.pl

functional properties of engineering materials also by applying alloying additives in an amount higher than that applied for a modification. For this purpose, the optimal concentration of the alloying additives, as well as the cooling rate, will be investigated, so that the final result will be a material with a good castability, which is important in casting of high precision elements; at the same time, these materials are characterized by the absence of defects in the form of porosity, and simultaneously with improved mechanical and operating properties [3–6].

When temperature increased slightly above 550 K, a phase transition of the β -phase into an fcc phase, denoted as α' , took place. Namely, diffraction lines of the β -phase abruptly disappeared for the alloys with $x(\text{Zn}) = 0.24$ and 0.40, while at the same time, diffraction lines of the α' -phase appeared at the high-angle side of all α -phase diffraction lines; the α -phase is now in a metastable equilibrium with α' -phase and therefore denoted as $\alpha(M/\alpha')$. The $\beta \rightarrow \alpha'$ phase transition takes place at 550 K. The DSC study of the alloy with $x(\text{Zn}) = 0.24$ gave the value of 555 K for the $\beta \rightarrow \alpha'$ phase transition (Fig. 6a), in line with XRD results. From the difference between the Bragg angles of the corresponding diffraction lines of the $\alpha(M/\alpha')$ - and α' -phases at 560 K, one could conclude that the unit-cell parameter of the α' -phase was about 0.9 % smaller than the one of the $\alpha(M/\alpha')$ -phase, due to a much higher Zn fraction contained in the α' -phase, the details of which were given in the previous paper [7]. The curve showing the temperature dependence of the relative difference of the unit-cell parameters of the $\alpha(M/\alpha')$ - and α' -phases ran parallel to the curve showing the temperature dependence of the difference in the Zn fractions contained in the two phases [7]. One may conclude that the relative difference in the unit-cell parameters between the $\alpha(M/\alpha')$ - and α' -phases and its dependence on temperature was dominantly determined by the difference between their Zn-fractions, and to a much smaller degree, by the coherency strains. At a given temperature, diffraction line intensities of the α' -phase were higher, when the $x(\text{Zn})$ was higher. The average intensity ratios of the corresponding diffraction lines of the $\alpha(M/\alpha')$ - and α' -phases were >1 for $x(\text{Zn}) = 0.24$ and <1 for $x(\text{Zn}) = 0.40$ at ≈ 560 K [7].

The ZA27-based alloys fall in the hypereutectoid range of the Zn–Al phase diagram. The unmodified alloy, ZA1, comprises primary α dendrites surrounded by the eutectoid (αAl) $\downarrow\leftarrow$ (Zn). The optical microstructures of all the as-cast alloys are given elsewhere. The addition of Ti results in rosette-shaped dendrites, whereas that of Sr results in dendrites with increased curvature. In the unmodified alloy, the zinc-rich matrix is anodic (more positive potential) with respect to the aluminium-rich dendrites. The corrosion product is formed by the same reaction as that in ZA1. Subsequently, the hydroxide forms a protective layer on the

surface of the metals and is expected to prevent or reduce further dissolution in the later stages. In the case of alloys, ZTiB1 and ZSr1, the mechanisms of corrosion and the corrosion product remain the same as in the other alloys [8].

The Al_2Sr phase is a homogeneous one, with an orthorhombic structure, with cell structure parameters being $a = 0.484$, $b = 0.792$ and $c = 0.799$ nm [9].

The addition of copper results in an increase in strength of the alloy; however, the material will suffer dimensional instability over a period of time at ambient temperature [10].

Both gravity casting and squeeze casting were carried out previously on a zinc alloy (ZA3) with different casting temperatures. Tensile, impact and density measurements were conducted. It was found that generally, samples taken from the bottom of the squeeze casting mould gave higher tensile strength, higher impact strength and higher density values. This study was carried out to determine the effect of solidification time on the mechanical properties of the castings. Two analytical methods were used: a steady-state heat flow model and Garcia's virtual model. It was found that similar results were obtained with both analytical methods. Casting samples taken from the lower part of the squeeze casting mould were found to have a significantly shorter solidification time. For both types of alloys, it was found that generally the shorter the solidification time of the casting, the higher are its density, impact energy, yield strength and ultimate tensile strength (UTS). This study has therefore contributed to a better understanding of the mechanical properties obtained previously from different casting processes [11].

Tensile, impact and density tests were carried out on the specimens. It was found that casting temperature had its effects on the mechanical properties of both gravity cast and squeeze zinc alloys. The best temperature to gravity cast the aluminium alloy and the zinc alloy was 460 °C, in both cases. However, for the squeeze casting of the zinc alloy, the best temperature was again 460 °C [2].

The microstructure of the ZnAlCu solder consisted of primary ε -phase, dendritic η -phase and eutectic/eutectoid α - η phases. However, the fraction of each phases varied as a function of the alloying content. As the Al and Cu contents increased, the α - η eutectic/eutectoid phases increased, thereby resulting in the increases of Vickers hardness and tensile strength [12].

The maximum segregation zone of the eutectic through the part section corresponds to the zone of final solidification point. The concentration of eutectic through the section changes depending on the initial mould temperature, pouring temperature and cooling rate. A high cooling rate reduces the rate of change in eutectic concentration across the section. The distance separating the maximum

segregation zone from the inner and outer faces of the casting can be controlled by controlling the ratio between the speeds of the solidification fronts advancing from opposite sides. The microstructure obtained becomes finer as the cooling rate increases. The structure of eutectic changes according to the cooling rate, which may be granular or lamellar [13].

The effects of Mg and RE additions on the microstructural evolution of a modified zinc alloy ZA27 during isothermal holding at semi-solid temperature of 460 °C have been studied using optical microscope and scanning electron microscope. Results show that these two elements both decrease the coarsening rate of solid primary particles, and improve the uniformity of particle size. The addition of Mg greatly decreases the solid fraction, and then increases the distance between particles. However, the element of RE mainly concentrates at the liquid regions between particles, and hinders both the atom diffusion and the welding of contact particles. In addition, the behaviours of particle coarsening of these two alloys, together with that of the Zr-added ZA27 alloy without the other elements, obey the LSW law after the three semi-solid systems reach their solid–liquid equilibrium states. The additions of these two elements have no visible effect on the shape factor of particles [14].

Materials and experimental procedure

The effects of cooling rate on the crystallization kinetics and the microstructure of the cast ZnAlCu alloys were investigated based on the model casts (Table 1) also with strontium addition.

The casts were performed in resistance furnace in chamotte graphite crucible, which were cast into metal moulds using ceramic filters. Mass concentration of the alloy after casting with Sr addition was confirmed by the chemical composition analysis carried out using the procedure OES ICP on the device, ULTIMA 2 Jobin-YVON.

From the material cast into the metal moulds, samples for thermo-derivative analysis were prepared with 30-mm diameter and a height of 35 mm. Holes were made in the samples for thermocouples, in the place where a thermal centre for this type of sample geometry can occur. The

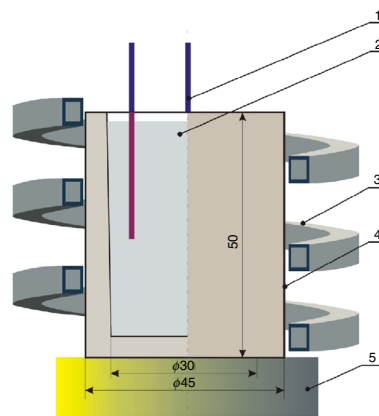


Fig. 1 Scheme of the heating and cooling system of the UMMA platform [1, 5] with the positioning of the thermocouples as well as the size of the samples for thermo-analysis: 1 thermocouple, 2 sample, 3 coil-cooling nozzles assembly, 4 crucible, 5 sampler isolation

investigated samples have masses of 160 ± 3 g for this type of geometric dimensions. The thermo-derivative analysis for the investigated alloys with alloying additives was performed using the graphite crucible of the metallurgical UMMA simulator (Universal metallurgical Simulator and Analyzer) equipped with dedicated software for control and calculation. Temperature measurement was carried out using a K-type thermocouple. The samples were cooled down slowly as well as with forced cooling using compressed argon (Fig. 1).

Microstructural investigation was performed using scanning electron microscope, Zeiss Supra 35, with the accelerating voltage of 5–25 kV, on properly prepared metallographic samples taken from the material melted in graphite crucibles and cooled at a suitable, correct DTA cooling rate for the DTA analysis.

The examinations of thin foils microstructure and phase identification were made on the JEOL 3010CX transmission electron microscope (TEM), at the accelerating voltage of 300 kV using selected area diffraction (SAD) method for phase investigations. The diffraction patterns from the TEM were solved using a dedicated computer software ‘Eldyf’.

TEM specimens were prepared by cutting thin plates from the material. The specimens were ground down to foils with a maximum thickness of 80 μm before 3-mm-diameter discs were punched from the specimens. The discs were further thinned by ion milling method with the Precision Ion Polishing System (PIPSTM), equipped with ion milling device model 691 supplied by Gatan until one or more holes appeared. The ion milling was done with argon ions, at an accelerating voltage of 15 kV, at angles of ca. 3.5°.

Table 1 Chemical composition of the model casts

Sample designation	Elements included in the chemical composition of the model casts
Cast 1/B/	ZnAlCuSr/content % mass./—Al 0,96; Cu 1; Sr 1,02; rest Zn
Cast 2/G/	ZnAlCu/content % mass./—Al 0,98; Cu 1; rest Zn

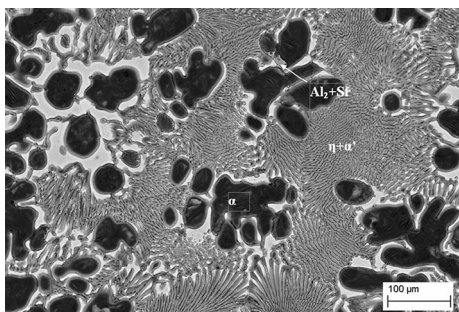


Fig. 2 Microstructure of the ZnAlCu alloy with Sr addition and cooled at the rate of $0.1 \text{ }^\circ\text{C s}^{-1}$

Investigations concerning the chemical composition of the alloy structure were performed using scanning electron microscope (SEM) Zeiss Supra 35 equipped with energy-dispersive spectrometer (EDS) supplied by Oxford. The investigations results concern the analysis of the material composition on the material's surface.

Results and discussion

In Figs. 2–5, the microstructures of the ZnAlCu alloys cooled with rates of ca. 0.1 and $1 \text{ }^\circ\text{C s}^{-1}$, also after addition of strontium, are presented. The desired cooling rate of $1 \text{ }^\circ\text{C s}^{-1}$ was obtained by cooling of the alloy from the temperature of $450 \text{ }^\circ\text{C}$ with argon flowing through the cooling nozzle placed in the inductor. After Sr addition, a lack of η phase on the boundary of the α phase dendrites was also found (Fig. 6), which is also observed on the derivative solidification curve of the alloy with Sr addition (Figs. 7, 8). Increase in the cooling rate causes microstructural refinement and morphological change of the α phase (Figs. 3, 5). In Figs. 9 and 10, the cooling curves and derivative curves of the ZnAlCu alloy with the marked characteristic points the crystallization of the phases and $\eta + \alpha$ eutectics are presented. In Table 2, the description of the characteristic points of the crystallised ZnAlCu alloy is presented. In Figs. 7 and 8, the cooling curves and derivative curves of the Sr-added ZnAlCu alloys are shown. In Table 3, the description of the characteristic points of the crystallised alloy after addition of the additives is presented. In Figs. 7 and 8, there is visible a lack of inflection points on the derivative curves of η phase crystallization. On the derivative curves, solid-state transformations of the phase, $\alpha \rightarrow \alpha'$, are not revealed.

Based on the thermo-derivative diagram, a double peak corresponding to the Al- α phase solidification can be recognized, as well as the Zn phase solidification, which is revealed as a white Zn—areas on the pictograms presented in the microstructure (Figs. 4, 5).

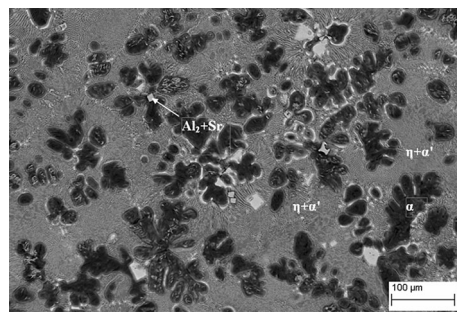


Fig. 3 Microstructure of the ZnAlCu alloy with Sr addition and cooled at the rate of $1 \text{ }^\circ\text{C s}^{-1}$

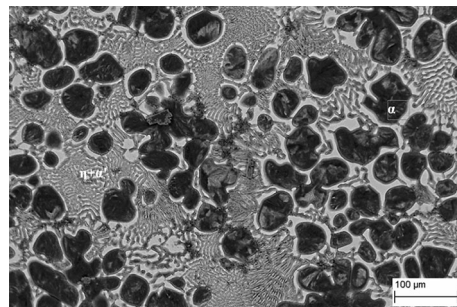


Fig. 4 Microstructure of the ZnAlCu alloy cooled at the rate of $0.1 \text{ }^\circ\text{C s}^{-1}$

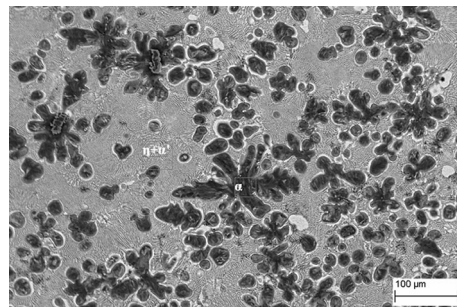


Fig. 5 Microstructure of the ZnAlCu alloy cooled at the rate of $1 \text{ }^\circ\text{C s}^{-1}$

Based on the transmission electron microscopy carried out, investigation results are presented in Fig. 6, which confirm the occurrence of the Al_2Sr phase present in the investigated Zn alloy matrix. For the investigated zinc alloy, a crystalline microstructure of the alloy after the controlled solidification process was detected. In Fig. 6a, the microstructure of the Zn alloy using the bright-field technique is shown, which can help in determining the grain size of the Zn subgrains, which can be determined in sizes up to $50 \text{ }\mu\text{m}$. Because of smaller crystalline structure, alloy could have also better mechanical properties.

For phase determination of the structure of the surface layer, diffraction pattern analysis of the investigated areas has allowed us to identify the Zn η phase (Fig. 6b) as a

Fig. 6 **a** Zn–Sr grains in the investigated alloy, bright field. **b** Diffraction pattern of the area presented on **a** with the solution of the diffraction pattern confirming the Zn matrix phase as well as the Al_2Sr phase with the zone axis $[3\text{-}2\text{-}1]$

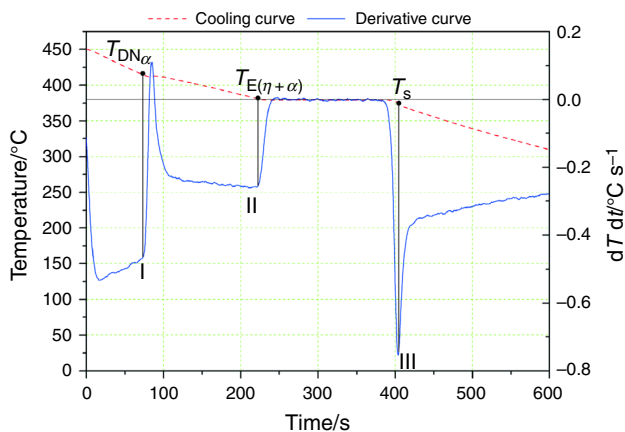
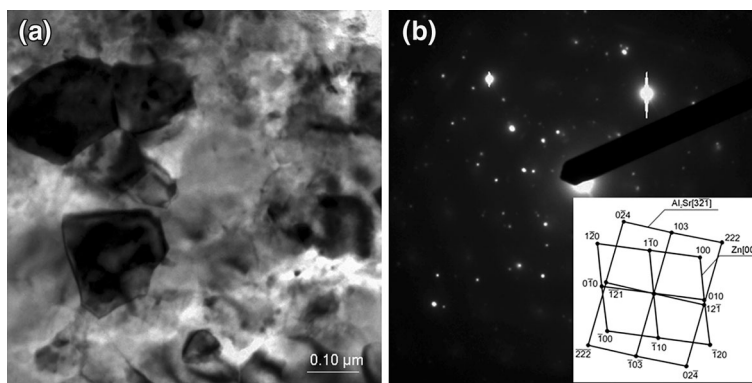


Fig. 7 Diagrams of the cooling curve and derivative curve of the ZnAlCuSr alloy cooled at the rate of 0.1 °C s^{-1}

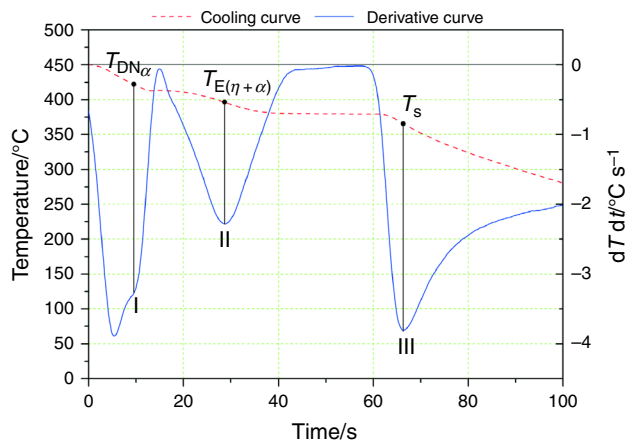


Fig. 8 Diagrams of the cooling curve and derivative curve of the ZnAlCuSr alloy cooled at the rate of 1 °C s^{-1}

hexagonal phase of the $P63/mmc$ space group with the d-spacing of $a = b = 0.2748$ and $c = 0.5167$ nm, which is greater than the lattice d-spacing found in the literature data for Zn phase being equal to $a = b = 0.2665$ and $c = 0.4947$ nm, i.e. ca. 3.1 % greater than a, b lattice parameters compared with the literature data and ca. 4.5 % greater than the c d-spacing compared with the literature data. So when the a and b d-spacings are placed in the statistically error region, so that the c d-spacing is already a measurable value which can be taken into account for the structural reinforcement of the Zn alloys with Sr addition.

The EDS line-wise analysis shown in Fig. 11 presents the chemical composition of the presented area in the form of line-wise analysis, and the changes of the aluminium and zinc compositions are clearly visible. In case of the copper distribution, the concentration fluctuations are present, and so it can be assumed that this element is more or less homogeneously distributed in the Zn alloy and is mostly dissolved in the matrix.

In Table 4, the temperature values at the beginning and at the end of the crystallisation of the alloy both before and

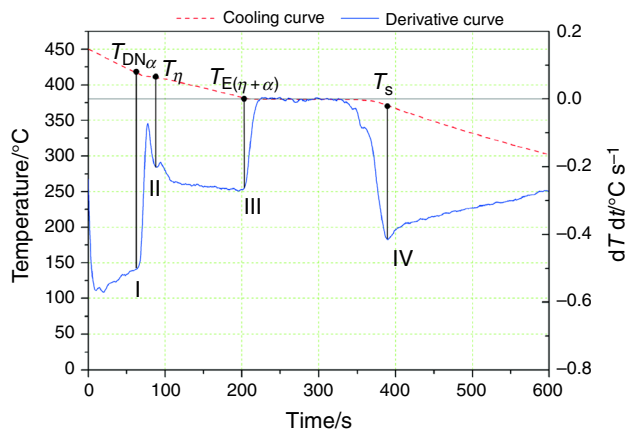


Fig. 9 Diagrams of the cooling curve and derivative curve of the ZnAlCu alloy cooled at the rate of 0.1 °C s^{-1}

after Sr addition are presented. Addition of strontium causes a decrease of the alloy’s overcooling. In Fig. 12, the changes of the fraction solid according to the temperature

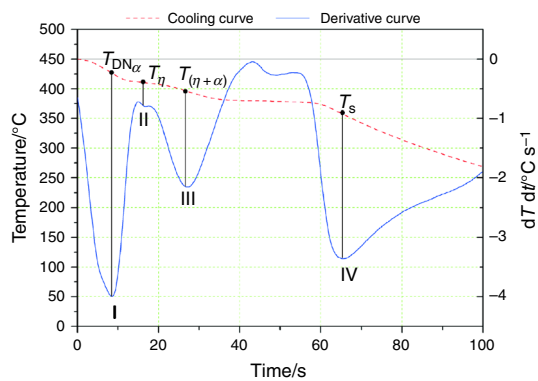


Fig. 10 Diagrams of the cooling curve and derivative curve of the ZnAlCu alloy cooled at the rate of 1 °C s^{-1}

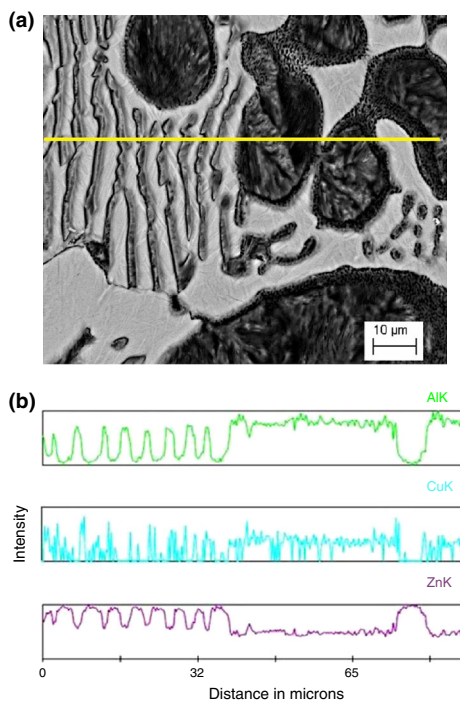


Fig. 11 Line-wise EDS analysis, carried out on the marked line in **a**, performed for Al, Cu and Zn in **b**

of the solidifying alloy and the cooling rate or Sr addition are presented.

Conclusions

Increase in the cooling rate causes microstructure's refinement and change in the morphology of α phase dendrites. After the addition of strontium, of a higher

Table 2 Description of the crystallization points of the phases and eutectics

Point on the graph on Figs. 9 and 10	Description
I	α phase growth temperature
II	Temperature of η phase growth
III	Nucleation temperature of the $\eta + \alpha$ eutectics
IV	T_S temperature of the crystallization end

Table 3 Description of the crystallisation points of the phases and eutectics

Point on the graph on Figs. 7 and 8	Description
I	α phase growth temperature
II	Nucleation temperature of the $\eta + \alpha$ eutectics
III	T_S temperature of the crystallization end

Table 4 Temperature values of crystallisation of phases and eutectics of the Zn alloy

	$T_{DN}/\text{°C}$		$T_S/\text{°C}$	
	$0,1\text{ °C s}^{-1}$	1 °C s^{-1}	$0,1\text{ °C s}^{-1}$	1 °C s^{-1}
ZnAlCu	415,5	419,2	370,5	358,8
ZnAlCuSr	415,9	420,5	372,2	365,9

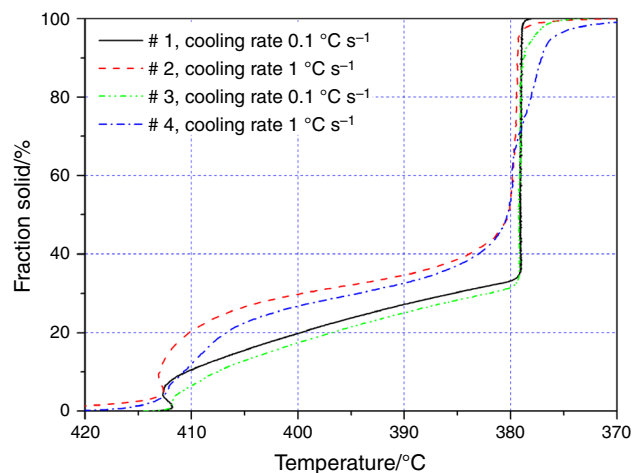


Fig. 12 Fraction solid of the Zn alloy cooled with a rate of 0.1 °C s^{-1} and 1 °C s^{-1} : #1, #2—ZnAlCuSr; #3, #4—ZnAlCu

amount like that in case of an inoculation (modification), there is a lack of crystallization of the η phase at the α phase boundary. The addition of strontium acts also a substrate for the heterogeneous nucleation changing the

crystallization kinetics, which is visible on the derivative curves, as well as analyzing the fraction solid diagram of the investigated alloys taking into account the chemical composition, alloying element's addition and the cooling rate of the alloy. In samples with strontium, there is no visible a clear point $\text{II} \rightarrow \text{T}_\eta$ (Figs. 9, 10) on the derivative curve, but solidification $\text{II} \rightarrow \text{T}_{\text{E}(\eta+\alpha)}$ (Figs. 7, 8).

As a result of the investigations carried out, it was found that there occur changes in the phase composition in the alloyed Zn cast alloy, concerning mainly the occurrence of the Al_2Sr phase. TEM investigations have allowed us also to determine the changes in the Zn grains lattice parameters like the d-spacing of $a = b = 0.2748$ and $c = 0.5167$ nm, which is greater than the lattice d-spacing according to the references for Zn phase being equal to $a = b = 0.2665$ and $c = 0.4947$ nm. The differences are ca. 3.1 % larger in case of “a”, “b” lattice parameters than the literature data and ca. 4.5 % greater in the case of the “c” d-spacing than the literature data.

The revealed microstructure based on the bright-field TEM technique investigations of which the Zn alloy consists, lead to the conclusion that the determined grain size of the Zn subgrains, is equal ca. 50 μm . Therefore, small crystalline structure should have a high influence on the mechanical properties enhancement of the produced alloy. It is also worth mentioning that the Al_2Sr phase has approximately the same size as the Zn subgrains.

Acknowledgements This research was funded by the Science Centre Nacional No. 2640/B/T02/2011/40 headed by Dr. Beata Krupińska.

Open Access This article is distributed under the terms of the Creative Commons Attribution License which permits any use, distribution, and reproduction in any medium, provided the original author(s) and the source are credited.

References

1. Dobrzanski LA, Krupinski M, Labisz K, Krupinska B, Grajcar A. Phases and structure characteristics of the near eutectic Al-Si-Cu alloy using derivative thermo analysis. *Mater Sci Forum*. 2010;638–642:475–80.
2. Yang LJ. The effect of casting temperature on the properties of squeeze cast aluminium and zinc alloys. *J Mater Process Technol*. 2003;140:391–6.
3. Kierkus WT, Sokolowski JH. Recent advances in cooling curve analysis: a new method for determining the ‘base line’ equation. *AFS Trans*. 1999;107.
4. Krupinski M, Dobrzanski LA, Sokolowski J, Kasprzak W, Byczynski G. Methodology for automatic control of automotive Al-Si cast components. *Mater Sci Forum*. 2007;539–543:339–44.
5. Krupiński M, Labisz K, Dobrzański LA, Rdzawski Z. Derivative thermo analysis of the Al-Si cast alloy with addition of rare earths metals. *Arch Foundry Eng*. 2010;10(1):79–82.
6. Tanski T, Dobrzanski LA, Cizek L. Influence of heat treatment on structure and properties of the cast magnesium alloys. *Adv Mater Res*. 2007;15–17:491–6.
7. Skoko Ž, Popović S, Štefanić G. Microstructure of Al-Zn and Zn-Al alloys. *Croat Chem Acta*. 2009;82(2):405–20.
8. Choudhury P, Das S. Effect of microstructure on the corrosion behaviour of a zinc–aluminium alloy. *J Mater Sci*. 2005;40:805–7.
9. Alcock CB, Itkin VP. The Al-Sr (aluminum-strontium) system. *Bull Alloy Phase Diagr*. 1989;10(6):624–30.
10. Mazhar AA, Salih SA, Gad-Allah AG, Tammam RH. Corrosion inhibition of Zn-Al-Cu alloy by 2-aminothiazole. *JMEPEG*. 2008;17:260–70.
11. Yang LJ. The effect of solidification time in squeeze casting of aluminium and zinc alloys. *J Mater Process Technol*. 2007;192–193:114–20.
12. Kang N, Na HS, Kim SJ, Kang CY. Alloy design of Zn–Al–Cu solder for ultra-high temperatures. *J Alloys Compd*. 2009;467:246–50.
13. Balout B, Masounave J, Songmene V. Modeling of eutectic macro segregation in centrifugal casting of thin walled ZA8 zinc alloy. *J Mater Process Technol*. 2009;209:5955–63.
14. Chen TJ, Hao Y, Sun J, Li YD. Effects of Mg and RE additions on the semi-solid microstructure of a zinc alloy ZA27. *Sci Technol Adv Mater*. 2003;4:495–502.